Journal of Asian Earth Sciences 62 (2013) 547–560

Contents lists available at SciVerse ScienceDirect

Journal of Asian Earth Sciences

journal homepage: www.elsevier.com/locate/jseaes

Controls on seasonal variations of silicate weathering and CO_2 consumption in two river catchments on the NE Tibetan Plateau

Fei Zhang [a,b], Zhangdong Jin [a,c,*], Fuchun Li [d], Jinmin Yu [e], Jun Xiao [a]

[a] State Key Laboratory of Loess and Quaternary Geology, Institute of Earth Environment, Chinese Academy of Sciences, Xi'an 710075, China
[b] University of Chinese Academy of Sciences, Beijing 100039, China
[c] School of Human Settlement and Civil Engineering, Xi'an Jiaotong University, Xi'an 710049, China
[d] College of Resources and Environmental Science, Nanjing Agricultural University, Nanjing 210095, China
[e] Research School of Earth Sciences, Australian National University, Canberra, ACT 0200, Australia

ARTICLE INFO

Article history:
Received 11 July 2012
Received in revised form 30 October 2012
Accepted 1 November 2012
Available online 15 November 2012

Keywords:
Weathering
Erosion
Climate
Lithology
CO_2 consumption
Seasonal variation

ABSTRACT

Water samples from the Buha and Shaliu Rivers, located on the semi-arid northeastern Tibetan Plateau, were collected weekly over a one year period. The major ionic compositions of water samples were measured and the daily contents of suspended particulate material (SPM) were monitored in both rivers in order to investigate the influence of lithology, climate and physical erosion on seasonal silicate weathering. In the Shaliu River, weathering of trace amounts of calcite contributes more than 50% of the Ca^{2+} and HCO_3^- to the river water. Through high-resolution variations of Ca^{2+} concentrations and elemental ratios, the signal of carbonate precipitation is captured at the end of monsoon in this river. The measured physical erosion rate is only 8.7–16.0 mm/kyr in this semi-arid region, which is 2–3 orders of magnitude lower than that in the Himalaya and nearby regions.

In contrast with several orders of magnitude in seasonal variations of silicate weathering rates in both catchments, the distinct lithology between the catchments only leads to a 15 times difference of annual net CO_2 consumption. The correlation analysis shows that seasonal silicate weathering is strongly dependent on water discharge in the semi-arid area. The most important observation is that, unrecognized by the previous studies, both physical erosion rate and air temperature exhibit two distinct trends with silicate weathering rates (and net CO_2 consumption) during the years. The two trends might suggest that temperature plays a more important role on the CO_2 consumption rate before the mid-monsoon under a condition of low water discharge than that after the monsoon with a high water discharge. During the period before the mid-monsoon, the relationship between temperature and silicate weathering rate exhibits higher activation energy than after the mid-monsoon, suggesting a greater dissolution of uneasily weatherable minerals from groundwater, frozen soil, and/or dust input. The relationship between erosion and weathering during the period before the mid-monsoon indicates a faster increase of silicate weathering rate, because freezing erosion produces large amount of high surface area minerals.

1. Introduction

Over geologic time scales, chemical weathering of silicate rocks is thought to regulate global climate through the uptake of atmospheric CO_2 (Walker et al., 1981; Berner et al., 1983; Berner and Kothavala, 2001). During the past decades, sustained attention has been focused on factors governing silicate weathering rates, such as lithology (Meybeck, 1986; Bluth and Kump, 1994; Edmond and Huh, 1997; Huh et al., 1998a), climate (White and Blum, 1995; Singh et al., 2005; Tipper et al., 2006; Wolff-Boenisch et al., 2009; Clow and Mast 2010), and physical erosion (Gaillardet et al., 1999; Huh and Edmond, 1999; Millot et al., 2002; Riebe et al., 2003; West et al., 2005). The relationship between these factors and silicate weathering, however, remains controversial. White and Blum (1995) proposed that climate, but not lithology and physical erosion, is the critical factor on controlling weathering by investigating their relationships in 68 small, mono-lithologic basins distributed around the world, whereas some found a weak or no correlation between temperature and weathering (Huh and Edmond, 1999; Riebe et al., 2004; Hagedorn and Cartwright, 2009). The importance of physical erosion has been highlighted by several recent studies that a linear relationship exists between rates of physical erosion and chemical weathering (e.g. Riebe et al., 2004; Hren et al., 2007; Hagedorn and Cartwright, 2009). Others observed a power function relationship between them (Gaillardet

* Corresponding author at: State Key Laboratory of Loess and Quaternary Geology, Institute of Earth Environment, Chinese Academy of Sciences, Xi'an 710075, China.
E-mail address: zhdjin@ieecas.cn (Z. Jin).

1367-9120/$ - see front matter © 2012 Elsevier Ltd. All rights reserved.
http://dx.doi.org/10.1016/j.jseaes.2012.11.004

et al., 1999; Millot et al., 2002; Singh et al., 2005; Qin et al., 2006). One emerging view argued that their relationship is not a simple linear correlation, i.e. under supply-limited conditions, chemical weathering is in linear increase with physical erosion, whereas under kinetically-limited conditions, the relationship becomes less linear (West et al., 2005; Gabet and Mudd, 2009). Further study is required to test the responses of chemical weathering to these controlling factors under various conditions.

Recently, several studies have attempted to explore their potential relationship through collecting seasonal or time-series samples (including river water and suspended particulate material (SPM)) at regional and catchment scales (e.g. Viers et al., 2000; Singh et al., 2005; Qin et al., 2006; Tipper et al., 2006; Moon et al., 2007; Gislason et al., 2009; Wolff-Boenisch et al., 2009; Zhang et al., 2009; Clow and Mast, 2010; Jin et al., 2011). However, most of the time-series sampling density is not high enough to minimize the uncertainties for defining these controlling factors. For example, Noh et al. (2009) proposed that the lack of expected correlation between total dissolved solids (TDSs) and SPM could be due to the inadequate temporal sampling density. Similarly, Hren et al. (2007) ascribed the non-linear correlation between temperature and cations to the narrow temperature range of available samples. Therefore, more high-resolution sampling studies are still required to obtain accurate estimates.

In this study, we are trying to investigate whether and what degree chemical weathering rate is affected by the factors of climate, lithology and physical erosion in the semi-arid northeastern Tibetan Plateau, by using high-resolution sampling at catchments of the Buha and Shaliu Rivers. The two river catchments are adjacent to each other and share the same climatic changes. By contrast, the two rivers are underlain and surrounded by distinctive lithology. The Buha River catchment is dominated by late Paleozoic marine limestone, whereas the Shaliu River by Triassic sandstone and late Cambrian metamorphic rocks. Each of these two rivers is monitored by one hydrological station that provides daily hydrological data such as water discharge, precipitation, and SPM. In addition, these pristine catchments are the least impacted by the human activities. The distinctive geological settings and high density sampling of river waters provide an ideal case to assess the climatic influences on catchment erosion and weathering, and to compare lithologic controls on the two catchments under the same climatic conditions. At last, these two river catchments are located in a semi-arid region, where the detailed seasonal variations of erosion and weathering are still sparse.

2. Study areas

2.1. Geography and climate

The Buha and Shaliu Rivers are located within the Lake Qinghai catchment on the northeastern Tibetan Plateau with an elevation of 3194 m at the river mouth (Fig. 1). As the largest river within the catchment, the Buha River has a length of 286 km and drains an area of 14,337 km^2. It sources from the Shule South Mountain (Qilian Mountains) where the mean elevation is >4600 m with glaciers. The water discharge of the Buha River was 10.05×10^8 m^3 in 2007, with its daily discharge varying from 2 m^3/s in February to 220 m^3/s in August (Fig. 2b) (Jin et al., 2011). The Shaliu River, second largest river feeding Lake Qinghai, drains an area of 1442 km^2, with a length of 109.5 km. It originates from the Datong Mountain at an elevation up to 5200 m (LZBCAS, 1994). The water discharge of the Shaliu River was 4.23×10^8 m^3 in 2009, with its daily discharge ranging from 0.1 m^3/s in February to 107 m^3/s in July (Fig. 2e).

The climate over the two rivers catchments was same (Fig. 2) and was characterized by windy-dry spring, rainy summer, and cold-snowy winter in both 2007 and 2009. Strong wind carrying eolian dust generally occurs in springtime (Chen et al., 2008). In

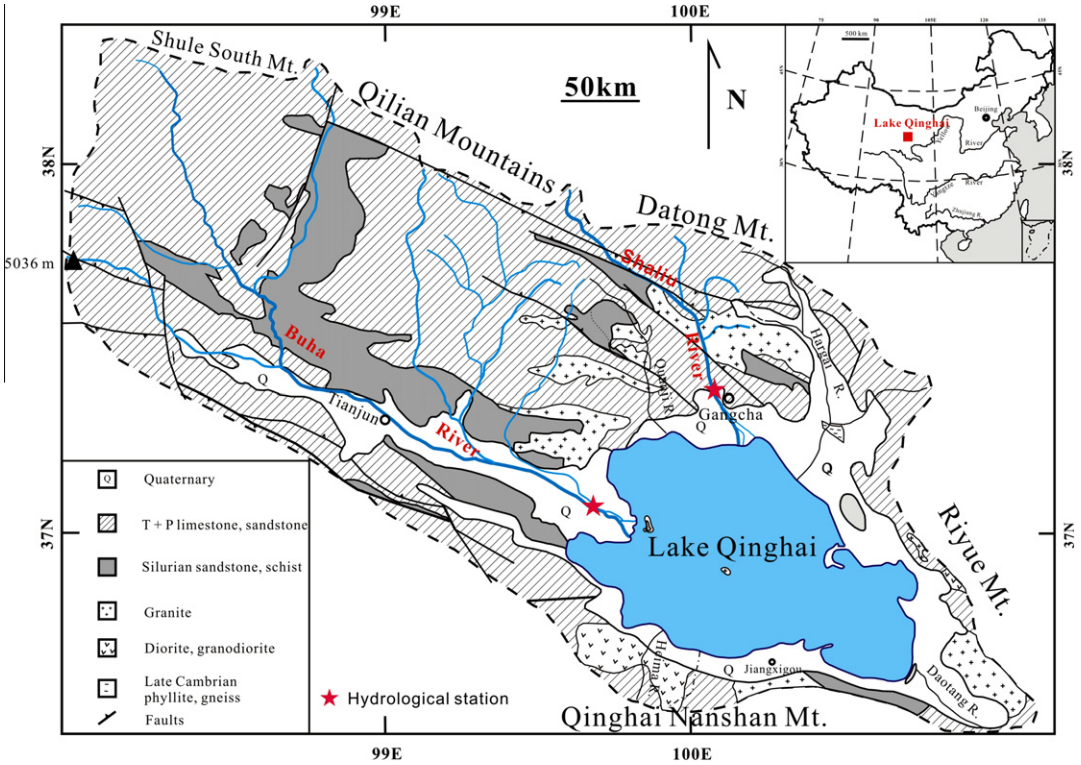

Fig. 1. Sketchy geologic map of the Lake Qinghai catchment on the northeastern Tibetan Plateau (modified after Jin et al. (2011)). The Buha River is on the northwest of the lake, and the Shaliu River on the north. The Buha and Shaliu hydrological stations are marked by red stars. Inserted map showing the location of Lake Qinghai. (For interpretation of the references to colour in this figure legend, the reader is referred to the web version of this article.)

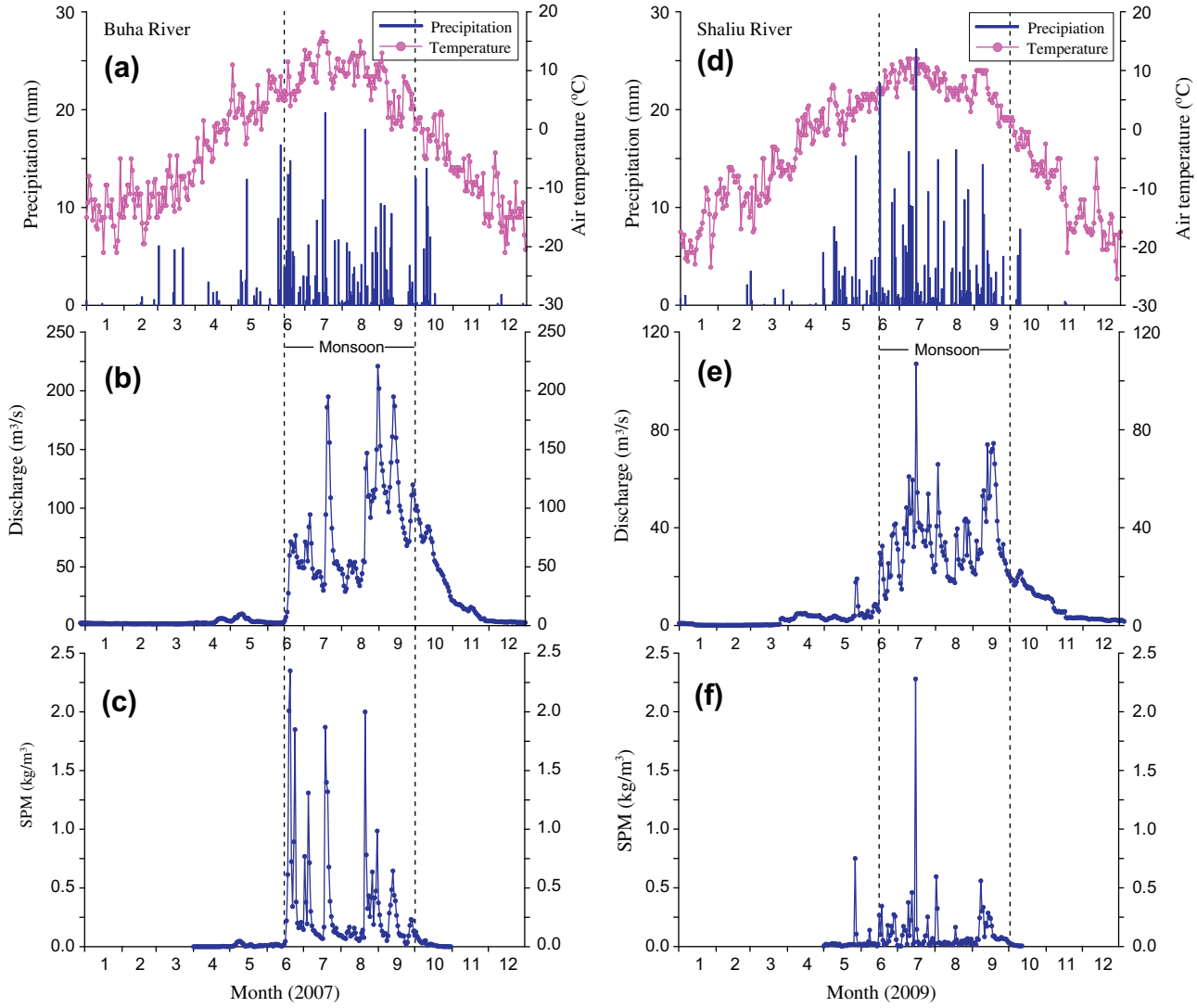

Fig. 2. Daily variations of air temperature, precipitation, water discharge and suspended particulate material (SPM) content in the Buha River in 2007 and in the Shaliu River in 2009. These data show apparent seasonal variations. The air temperature was above 0 °C from May to October. The main precipitation, discharge and SPM were occurred during the monsoon seasons in both the Buha and Shaliu Rivers. The SPM samples were only collected from April to October in the Buha River, and from May to October in the Shaliu River, respectively.

the Buha River catchment, the total precipitation was 389.8 mm in 2007, and the mean daily air temperature during a year ranged from −20.5 °C to 16.5 °C (Fig. 2a). In the Shaliu River catchment, the annual precipitation was 431.0 mm in 2009, with the mean daily air temperature ranging from −25.5 °C to 12.0 °C (Fig. 2d). On average, about 90% of the precipitation occurred from May to September (1961–2001) as same as in both 2007 and 2009, resulting in 75–85% water discharge during this period at both catchments. Nearly no precipitation occurred from December to February. During spring season (from March to June), although the precipitation is still in the form of snow, the increasing air temperature lead to the melting of glacier, ice and snow, and hence produces increasing water discharge. The annual average potential evaporation was approximately 1650 mm and 1463 mm at the Buha and Shaliu Rivers, respectively. Highest monthly air temperature was in July and coldest in January. From middle October to late April, the air temperature was generally below 0 °C. The meteorological and hydrological data above mentioned were provided by the Buha and Shaliu River hydrological stations. The vegetation is dominated by semi-arid climate species including montane shrub, alpine steppe, and high-alpine meadow in both catchments (LZBCAS, 1994).

2.2. Geology

Situated on the southern edge of the Qilian fold belt, Lake Qinghai is an intermountain basin surrounded by Mts. Riyue Shan, Qinghai Nan Shan, Shule Nan Shan, and Datong Shan on the east, south, northwest and north, respectively (Chen et al., 2008). The lake was formed during late Cenozoic neo-tectonic activities and controlled by a triple junction of NWW, NNW and S–N trending tectonic units. On the north of the lake, the Mt. Datong Shan is NNW strike with bedrock uncovered (Bian et al., 2000).

The Buha River catchment comprises hummocky terrain of predominantly Permian marine limestone and sandstones, Silurian sandstones and schist (Fig. 1). Mesozoic granites outcrop in the northern part of the catchment near the shore of Lake Qinghai. The river has created fluvial plains and delta along the western shores. Within the catchment, some modern glaciers exist on mountains in the upper Buha River drainage basin (Jin et al.,

2011). In the Shaliu River catchment, Triassic sandstone and schist outcrop in the west of Gangcha County, Late Cambrian metamorphic rocks (schist and gneiss) in the east, and granite in the north (LZBCAS, 1994).

3. Samples and analysis

River water samples were collected weekly at the Buha River hydrological station in 2007 and the Shaliu River station in 2009. The stations are both located in the low reaches of the rivers where waters from tributaries converge (Fig. 1). The SPM, water discharge, precipitation and temperature were monitored daily at the hydrology stations. The water discharge was monitored twice per day, and when in flood periods, the monitoring frequency was increased to 4–5 times 1 day. In total, thirty-one water samples of rain and snow were also collected within the two catchments during 2007 and 2010.

Water samples (including rain and snow after melted) were *in situ* filtered on collection through 0.2 μm Whatman® nylon filters. For cation analysis, 60 mL filtered water of each sample was stored in a pre-cleaned polyethylene bottle and was acidified to pH < 2 using 6 M quartz-distilled HNO_3. For anion measurements, 30 mL filtered sample was stored but not acidified. Bottles were wrapped parafilm strip around the closure to prevent any leakage. Temperature and pH were measured at the sampling sites synchronously. All samples were kept chilled at 4 °C until analysis. Major rocks, include limestone, granite, sandstone, clastic rock, schist and gneiss, were collected within the two catchments for element composition measurements.

Major cations of the water samples were analyzed by Leeman Labs Profile ICP-AES at State Key Laboratory of Lake Science and Environment, with a reproducibility of 1–2%. Major anions were determined by a Dionex-600 ion chromatography at Institute of Earth Environment, Chinese Academy of Sciences (IEECAS). The average reproducibility was 0.5–1% (2σ). Alkalinity (expressed as HCO_3^- in Tables 1 and 2) was measured by Gran titration. Rock samples were analyzed for major elemental compositions by a wavelength dispersion X-ray fluorescence spectroscopy at IEECAS. Repeat analysis demonstrates a reproducibility of 2–5%.

4. Results and discussion

4.1. Physical erosion rate and seasonal variation

The time series physical erosion rate (PER) in both the Buha and Shaliu Rivers was obtained by daily SPM concentration multiplied water discharge. In this study, the daily SPM concentration was measured during the period from May to October. It is observed that the daily SPM concentration varies from <0.001 kg/m^3 in the dry season to 2.280 kg/m^3 in the monsoon in the Buha River, and from <0.003 kg/m^3 to 2.350 kg/m^3 in the Shaliu River. The PERs calculated by daily SPM are 16 mm/kyr in the Shaliu River and 8.7 mm/kyr in the Buha River catchment. These values are 2–3 orders of magnitude lower than PER in the High Himalaya (2700 mm/kyr) and that in the southern edge of the Tibetan Plateau (1200 mm/kyr) (Vance et al., 2003). An explanation for such low PER in the semi-arid area is the extremely low precipitation, because heavy monsoonal precipitation has been thought to act as a first-order control of rapid physical erosion in the Himalayas (Galy and France-Lanord, 2001).

The PER data exhibit significant seasonal variations in both the Buha and Shaliu Rivers. It varies from <1 tons/day in the dry season to 23,155 tons/day during the monsoon in the Buha River, and from <1 tons/day to 21,078 tons/day in the Shaliu River, respectively.

4.2. General characteristics of river water chemistry

River water pH, temperature, and major ion concentrations of the Shaliu River are listed in Table 1. The data of the Buha River were reported by Jin et al. (2011). Water temperatures of the Shaliu River varied from 0 °C to 15.7 °C in 2009, with the lowest values in January/December and the highest in July. All waters are alkaline with pH values between 8.17 and 8.67. The Normalized Inorganic Charge Balance (NICB) is used to estimate overall analytical uncertainties (Table 1). NICB is expected to be close to zero, unless one or more ions have been overlooked during analyses. With the exception of two samples with the NICB of −12.53% and 10.67% collected in the February, all samples from the Shaliu River are well balanced with NICB < ±10%. The TDS in the Shaliu River shows a factor of 2–3 variation, ranging from 208 mg/L in July to 573 mg/L in March (Table 1). The general properties of the Buha River (Jin et al., 2011) are similar to those of the Shaliu River.

The total molar cation concentrations follow an order of $Ca^{2+} > Na^+ \approx Mg^{2+} \gg K^+$ in the Shaliu River, and $Ca^{2+} > Na^+ > Mg^{2+} \gg K^+$ in the Buha River. The major cation is Ca^{2+}, contributing to 39–67% and 38–67% of TZ^+ in the Shaliu and Buha Rivers, respectively. The second major cation is Na^+, accounting for 9–25% and 11–37% of the total cation charges in the Shaliu and Buha Rivers, respectively (Fig. 3a).

HCO_3^- is the most abundant anion, accounting for 64–87% and 60–77% of the TZ^- in charge equivalent units, in the Shaliu and Buha Rivers, respectively. The molar anion concentrations listed in Table 1 follow an order of $HCO_3^- > Cl^- > SO_4^{2-} > NO_3^- \gg F^-$. A ternary diagram (Fig. 3b) shows that most of the data cluster around the alkalinity apex leaning towards ($Cl^- + SO_4^{2-}$), with 12–35% and 22–36% of the total anion charges contributed from ($Cl^- + SO_4^{2-}$) in the Shaliu and Buha Rivers, respectively. This indicates that the evaporite dissolution and/or pyrite oxidation provide ($Cl^- + SO_4^{2-}$) to the rivers.

The abundant Ca^{2+} and HCO_3^- in both the Shaliu and Buha Rivers suggest that carbonate weathering dominates the water chemistry.

4.3. Temporal and spatial variations of major ions in river waters

Similar to the physical erosion processes, the water chemistry in both rivers shows significant seasonal variations (Fig. 4). During monsoon seasons, all of the major ions systematically decrease to the lowest values due to dilution by high water discharge. By contrast, these ions are concentrated during dry seasons when precipitation is at the lowest level of the years. In this case, the river discharge possibly comes partly from subsurface flow that has a longer water–rock contact time and thus greater dissolution of the solids.

It is noted that during the periods from late winter to spring, concentrations of major ions, particularly Na^+ and Cl^-, reach their highest values in both rivers (Fig. 4). Jin et al. (2011) ascribed these highest ion concentrations in the Buha River to the eolian dust input. In the Shaliu River, its slightly high major ion contents during the late winter might also be ascribed to the dust input, because the season was characterized by frequently dust storms. It is also observed that the relatively high major ion concentrations occurred during the autumn in the Shaliu River. This may be due to evaporation because ratios of ions remain constant (Figs. 3 and 4). For example, 11 samples from the Shaliu River collected from 6th September to 15th November show constant Cl/SO_4 of 0.9 and Mg/Na^* of 1.5 (Na^* was corrected by halite input) as TDS varied from 381 mg/L to 484 mg/L.

However, Ca^{2+} varies in an opposite trend in the autumn in the Shaliu River, showing decreased concentrations (Fig. 4a and b). A likely explanation is that Ca^{2+} was removed by the precipitation of secondary calcite. The calcite saturation index (CSI, Bethke and

Table 1
Dissolved major ions and calcite saturation index data of river waters from the Shaliu River sampled weekly in 2009.

Sample no.	Date (mm/dd/yy)	T[a] (°C)	pH	Ca^{2+} (μmol/L)	K^+ (μmol/L)	Mg^{2+} (μmol/L)	Na^+ (μmol/L)	Si (μmol/L)	F^- (μmol/L)	Cl^- (μmol/L)	NO_3^- (μmol/L)	SO_4^{2-} (μmol/L)	HCO_3^- (μmol/L)	TDS[b] (mg/L)	NCBI[c] (%)	CSI[d]
SL09-01	01/04/09	0.2	8.17	1512	193	867	1302	101	5.37	892	n.a.	651	3982	462	1.12	0.60
SL09-02	01/11/09	0.4	8.35	1621	45	723	1591	100	10.24	958	235	492	4326	487	−2.99	0.85
SL09-03	01/18/09	0.6	8.29	1795	39	767	1704	110	8.45	1018	242	525	4179	494	5.41	0.82
SL09-04	01/25/09	0.2	8.45	1634	41	734	1600	99	11.19	962	227	495	4375	490	−2.95	0.95
SL09-05	02/01/09	0.3	8.34	1624	43	725	1587	100	8.99	965	243	498	4375	491	−4.11	0.84
SL09-06	02/08/09	0.5	8.23	1503	192	889	1300	102	7.53	968	n.a.	708	4670	513	−12.53	0.72
SL09-07	02/15/09	5.5	8.54	1612	58	663	623	143	6.70	420	107	301	4129	408	−0.66	1.11
SL09-08	02/22/09	6.0	8.35	2132	56	849	1131	124	8.92	729	175	452	4572	501	10.67	1.07
SL09-09	03/01/09	6.1	8.50	969	53	899	1181	153	8.56	737	177	458	3490	393	−7.20	0.78
SL09-10	03/08/09	5.2	8.51	1538	42	592	530	130	6.18	345	96	270	4031	388	−3.87	1.05
SL09-11	03/15/09	6.3	8.60	2231	52	856	1131	130	12.06	753	186	454	5653	573	−2.12	1.41
SL09-12	03/22/09	6.4	8.54	1005	50	866	1131	145	8.56	698	175	439	3441	386	−5.62	0.84
SL09-13	03/29/09	9.5	8.41	1230	53	641	641	133	4.58	377	77	301	3294	338	1.81	0.84
SL09-14	04/05/09	9.8	8.49	1189	43	648	639	131	5.05	369	82	291	3441	344	−2.84	0.93
SL09-15	04/12/09	9.8	8.55	1737	47	698	617	131	2.01	384	94	308	4424	429	0.24	1.23
SL09-16	04/19/09	9.7	8.45	1126	29	450	420	88	2.48	225	46	214	2753	271	4.07	0.79
SL09-17	04/26/09	11.1	8.49	1271	30	490	459	86	4.42	254	62	223	3048	300	4.88	0.93
SL09-18	05/03/09	10.5	8.29	1206	36	476	537	82	4.05	267	52	236	2950	294	4.85	0.69
SL09-19	05/10/09	10.5	8.40	1201	30	465	462	77	3.24	239	47	212	3048	294	1.64	0.82
SL09-20	05/17/09	10.1	8.42	1117	28	415	420	71	1.93	162	48	222	2704	265	4.33	0.75
SL09-21	05/24/09	11.3	8.45	1121	28	412	418	69	3.11	159	61	220	2753	268	2.75	0.81
SL09-22	05/31/09	10.8	8.36	1104	31	398	403	70	1.72	147	24	202	2655	257	6.02	0.70
SL09-23	06/07/09	12.6	8.39	1103	32	396	409	71	1.79	159	33	208	2704	261	3.60	0.76
SL09-24	06/14/09	13.1	8.43	1117	28	410	415	70	2.06	158	32	212	2802	268	2.25	0.82
SL09-25	06/21/09	13.8	8.35	1108	32	397	409	71	1.74	160	27	200	2753	263	3.19	0.74
SL09-26	06/28/09	13.7	8.33	1119	31	406	412	71	1.73	160	30	207	2605	256	8.10	0.70
SL09-27	07/05/09	15.2	8.35	1112	31	404	409	71	1.94	166	49	209	2802	269	1.01	0.77
SL09-28	07/12/09	15.3	8.35	1119	31	408	416	71	1.86	161	29	209	2753	265	3.95	0.77
SL09-29	07/19/09	15.7	8.18	870	46	305	263	84	4.83	145	43	136	2163	208	1.20	0.42
SL09-30	07/26/09	15.2	8.34	1209	30	443	436	75	2.34	155	38	223	3146	296	-0.46	0.84
SL09-31	08/02/09	14.0	8.47	1240	30	439	450	76	2.48	157	44	215	3023	290	4.73	0.94
SL09-32	08/09/09	14.3	8.48	1293	37	448	419	80	2.86	173	33	211	3048	293	6.58	0.98
SL09-33	08/16/09	14.3	8.52	1368	31	488	471	86	3.63	186	89	250	3441	330	−0.11	1.08
SL09-34	08/23/09	16.1	8.41	n.a.	n.a.	n.a.	n.a.	n.a.	n.a.	n.a.	n.a.	n.a.	n.a.	n.a.	n.a.	n.a.
SL09-35	08/30/09	14.4	8.34	1068	45	513	516	98	2.74	165	50	260	2962	289	0.61	0.75
SL09-36	09/06/09	12.8	8.61	1520	42	626	605	114	4.15	218	55	272	3966	378	3.07	1.24
SL09-37	09/13/09	14.1	8.67	1603	53	743	722	134	4.48	268	65	321	4307	416	3.29	1.36
SL09-38	09/20/09	13.3	8.33	1132	101	867	832	150	5.61	343	90	399	3716	381	−0.43	0.82
SL09-39	09/27/09	10.9	8.56	1077	65	972	938	165	5.32	383	110	480	3751	396	−2.15	0.98
SL09-40	10/04/09	10.1	8.64	1379	61	868	845	165	5.54	326	80	379	4070	409	2.99	1.19
SL09-41	10/11/09	11.2	8.37	1226	86	875	834	156	4.75	337	176	393	3726	390	1.78	0.86
SL09-42	10/18/09	10.5	8.57	1393	50	725	701	127	4.52	259	67	324	3900	382	2.19	1.12
SL09-43	10/25/09	9.7	8.60	1608	62	888	838	149	6.12	336	79	394	4498	446	3.14	1.24
SL09-44	11/01/09	8.0	8.62	1464	54	771	736	135	5.37	279	70	346	4059	400	2.96	1.17
SL09-45	11/08/09	7.6	8.43	1301	81	885	834	155	5.40	339	85	484	3963	411	−1.35	0.91
SL09-46	11/15/09	7.3	8.65	1602	56	815	767	141	5.08	291	71	354	4866	458	−5.02	1.29
SL09-47	11/22/09	5.8	8.52	1725	46	708	599	121	7.42	300	61	223	4528	421	3.08	1.16
SL09-48	11/29/09	5.6	8.53	1735	60	687	605	118	6.06	306	65	233	4563	425	1.89	1.17
SL09-49	12/06/09	0.3	8.56	1743	35	614	453	107	3.98	231	53	206	4728	423	−4.36	1.14
SL09-50	12/13/09	0	8.58	1726	35	617	447	108	4.04	226	49	209	4001	377	9.09	1.09
SL09-51	12/20/09	1.6	8.56	1835	34	692	584	108	6.48	341	301	200	4215	419	7.21	1.13
SL09-52	12/27/09	1.8	8.55	1838	41	661	511	109	4.13	269	31	230	4591	423	3.53	1.16
SL09-53	01/04/10	1.9	8.46	1821	41	659	508	108	3.86	267	31	227	4579	421	3.12	1.07

n.a. – Not analyzed.
[a] *T* refers to water temperature when the samples were collected.
[b] Total dissolved solids.
[c] Normalized Inorganic Charge Balance (NICB) = $(TZ^+ - TZ^-)/TZ^+$, where $TZ^+ = Na^+ + K^+ + 2Mg^{2+} + 2Ca^{2+}$, $TZ^- = Cl^- + 2SO_4^{2-} + HCO_3^- + NO_3^-$ in μEq.
[d] Calcite saturation index was calculated using Geochemist's Workbench V.8.0 (Bethke and Yeakel, 2009).

Yeakel, 2009) shows that river waters are supersaturated with respect to calcite (Table 1). Furthermore, Fig. 5 indicates that Mg/Na^* ratios remain constant at 1.5, whereas Ca/Na^* ratios decrease from 3.5 to 2.1 during the autumn in the Shaliu River, suggesting removal of Ca^{2+} from river waters.

The differences of major ionic contents between two rivers over a one year period are higher Na^+, Cl^- and SO_4^{2-} concentrations in the Buha River than those in the Shaliu River, indicating a higher contribution of evaporite input to the Buha River. Meanwhile, higher Ca/Na^* and Mg/Na^* ratios in the Buha River waters (Fig. 5) suggest that the Buha River gains more carbonate weathering from its catchment than the Shaliu River, in response to a large area of limestone distribution within the Buha River catchment.

4.4. Sources of dissolved load

The potential major sources of dissolved ions into the river waters include (1) atmospheric deposition, (2) weathering of rock-forming minerals (silicates, carbonates, and evaporite), and (3) anthropogenic input. Considering the sparsely population, anthropogenic input is negligible in our study area. In this study, we adopt the forward model (Galy and France-Lanord, 1999; Noh

Table 2
Chemical compositions of rain and snow, sampled from the Buha River and Shaliu River catchments.

Sample no.	Date (mm/dd/yy)	Na^+ (μmol/L)	K^+ (μmol/L)	Ca^{2+} (μmol/L)	Mg^{2+} (μmol/L)	F^- (μmol/L)	Cl^- (μmol/L)	SO_4^{2-} (μmol/L)	NO_3^- (μmol/L)
5-F-01[a]	05/25/08	136	64	790	83	11.59	49	94	10
5-F-02[a]	06/22/08	51	9	313	26	n.a.	57	57	26
5-F-03[a]	06/27/08	133	22	761	58	0.65	111	49	20
5-F-04[a]	07/03/08	68	57	90	8	n.a.	34	71	34
5-F-05[a]	07/15/08	50	27	590	42	n.a.	34	31	16
5-F-06[a]	07/16/08	38	7	196	21	n.a.	13	25	7
5-F-07	07/18/08	99	46	579	44	n.a.	135	47	n.a.
5-F-08	07/21/08	172	142	68	6	1.89	20	43	5
5-F-09	07/28/08	122	126	65	5	0.86	31	61	1
5-F-10	09/06/08	18	14	43	4	n.a.	18	20	7
5-F-11	09/06/08	12	13	54	3	n.a.	10	10	1
5-F-12	09/09/08	23	13	59	8	n.a.	24	20	5
5-F-13	09/23/08	51	27	76	10	n.a.	32	61	16
5-F-14	09/25/08	68	30	101	16	n.a.	39	34	7
5-F-15	09/28/08	23	16	90	6	n.a.	14	18	16
Rain2	05/31/10	28	3	115	29	3.52	26	43	13
Rain3	07/04/10	50	89	102	28	4.69	182	48	0
Rain4	07/11/10	35	38	77	15	4.24	81	54	18
Rain5	07/15/10	51	32	160	32	4.88	44	75	n.a.
Rain6	08/04/10	62	72	97	39	5.22	80	100	22
Rain7	08/30/10	77	16	203	71	5.02	56	71	n.a.
rw-1	10/10/07	67	12	441	41	8.52	58	74	9
Rain1	03/03/10	95	21	242	44	n.a.	73	72	n.a.
Snow1	03/16/07	20	13	215	11	5.70	20	17	22
Snow2	10/11/07	18	14	130	14	4.31	34	22	0
Snow3	10/13/07	94	40	222	16	4.94	25	99	19
Snow4	01/27/08	313	123	356	100	6.45	216	92	95
Snow5	02/09/08	124	58	569	87	9.44	102	152	93
Snow6	04/21/08	254	21	415	38	n.a.	235	85	5
Snow7	10/10/08	19	14	60	6	n.a.	25	27	28
Snow8	11/06/08	11	6	48	7	n.a.	22	16	27

n.a. – Not analyzed.
[a] Data from Jin et al. (2011).

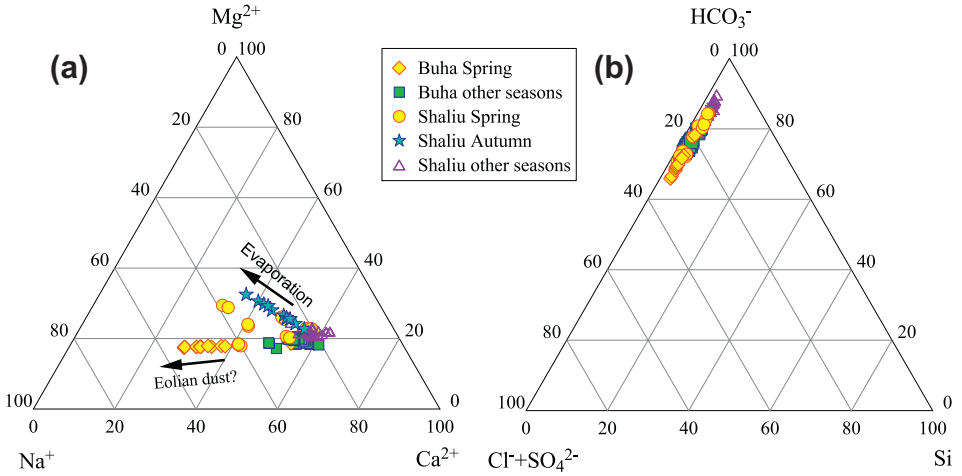

Fig. 3. Ternary diagrams for cations (a) and anions (b) of river water samples from the Buha and Shaliu Rivers, indicating dominance of Ca^{2+} and HCO_3^-. Samples close to Na^+ and (Cl^- + SO_4^{2-}) apexes in the spring season in the Buha River suggest a potential input of eolian dust (Jin et al., 2011), whereas the samples close to Na^+ and Mg^{2+} apexes in the autumn in the Shaliu River likely reflecting an evaporation effect.

et al., 2009) to calculate the fractions of weathering of different rocks after atmospheric input correction.

4.4.1. Atmospheric input

Some solutes in rainfall can constitute an important fraction of dissolved species appearing in surface waters (Meybeck, 1983). The aim of the atmospheric input correction is to quantify and subtract the portion of the elements carried by rainwater in the chemical compositions of the river water. Different methods for atmospheric input correction have been used (Meybeck, 1983; Stallard and Edmond, 1981; Grosbois et al., 2000; Millot et al., 2002; Das et al., 2005; Hren et al., 2007). The rainwater correction here is followed the method by Grosbois et al. (2000), as illustrated by the following equation:

$$X^* = (X/\mathrm{Cl})_{rain} \times \mathrm{Cl}_{ref} \quad (1)$$

where X^* refers to corrected concentration derived from rain water, and $(X/\mathrm{Cl})_{rain}$ refers to measured ion/Cl in rain water and Cl_{ref} is Cl^-

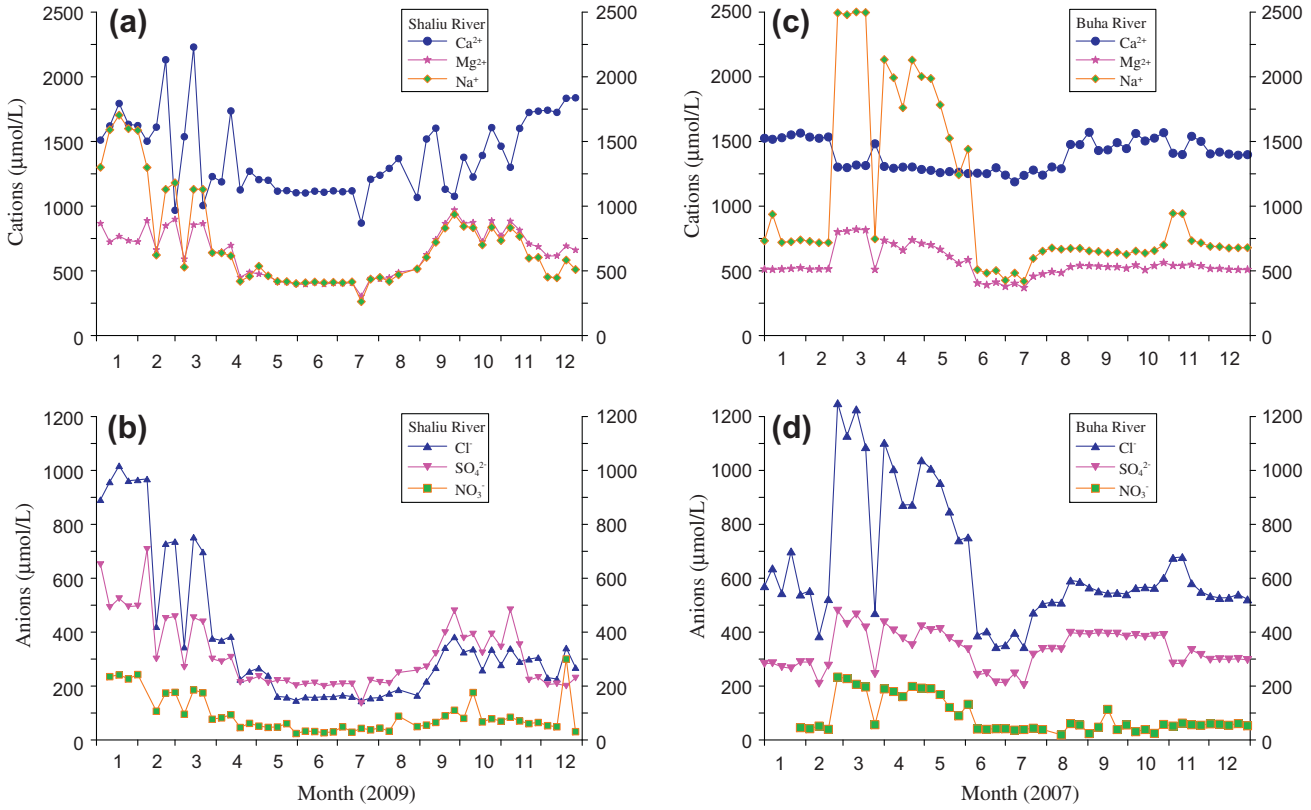

Fig. 4. Weekly variations in concentrations of major ions in the Shaliu and Buha Rivers, showing significant seasonal variations. The highest major ions are observed in the late winter and early spring, and the lowest in the monsoon period.

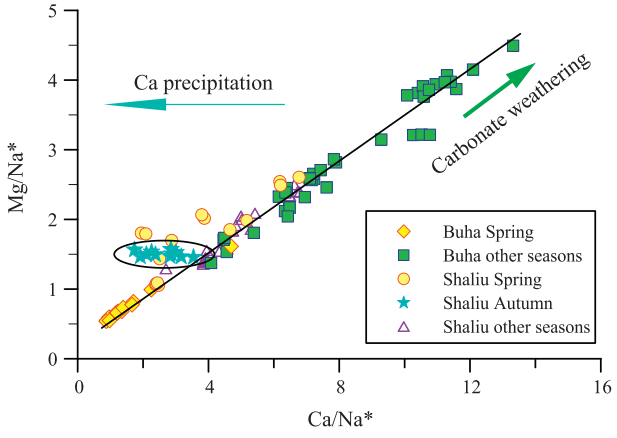

Fig. 5. Plot of Ca/Na^* versus Mg/Na^* in the Buha and Shaliu Rivers. Na^* was corrected by the halite input. The trend in the data indicates that more carbonate weathering occurred in the Buha River than in the Shaliu River, and that Ca^{2+} was removed in the Shaliu River in the autumn.

concentration derived from rainwater. The Cl_{ref} is calculated with average weighted Cl^- content of rain samples (Cl_{ave}) multiplied by concentration factor F, i.e. $Cl_{ref} = F^*Cl_{ave}$. The F value represents the concentration effect of evapotranspiration and is related to the total quantity of rainwater P (in mm) and the evapotranspiration process E (in mm) by the equation:

$$F = P/(P - E) \quad (2)$$

To better constraining seasonal atmospheric contributions, our rain samples are divided into two groups (Table 2). The first group is samples collected during monsoon seasons (May–September), and the remaining is the second group. Two reasons for doing this are as the follows. On the one hand, the water vapor sources of dry seasons are different from the monsoon seasons (Chen et al., 2008). During the monsoon seasons, warm and moist air mass is originated from the low latitudes ocean and brings most of annual precipitations, whereas rain in dry seasons is mainly controlled by cold continental high-pressure system (the Westerlies), which brings cold and dry air with frequent dust. On the other hand, as

Table 3
Chemical compositions of silicate rocks collected in the Buha River and Shaliu River catchments.

Catchment	Rocks	SiO_2 (wt.%)	Al_2O_3 (wt.%)	Fe_2O_3 (wt.%)	MgO (wt.%)	CaO (wt.%)	Na_2O (wt.%)	K_2O (wt.%)	Ca/Na (mol/mol)	Mg/Na (mol/mol)	Number of rocks
Buha River	Granite	69.73	13.83	3.29	1.61	2.91	2.56	3.18	0.63	0.49	$n = 5$
	Schist	68.45	14.12	3.90	1.49	1.71	2.57	3.71	0.37	0.45	$n = 7$
	Sandstone	79.04	8.90	1.85	0.89	1.41	2.04	2.30	0.38	0.34	$n = 4$
	High-grade metamorphic rock	66.96	15.45	3.76	1.42	1.92	4.05	3.74	0.26	0.27	$n = 11$
	Ratio range								0.47 ± 0.19	0.38 ± 0.11	
Shaliu River	Granite	71.03	13.30	2.95	0.95	2.14	2.45	4.32	0.48	0.30	$n = 2$
	Sandstone	77.20	10.10	2.57	1.50	1.07	2.55	1.24	0.23	0.46	$n = 2$
	Clastic rocks	68.99	11.47	4.45	1.81	2.94	2.36	1.69	0.69	0.60	$n = 2$
	Ratio range								0.48 ± 0.43	0.45 ± 0.16	

the study area is in the high altitude region (>3200 m), the air temperature is generally below 0 °C from October to April and the precipitations are in forms of snow and hail, while from May to September, the average monthly air temperature ranges from 3.5 to 11.5 °C and the precipitation is in form of rain.

Following the groups, the Cl_{ave} are 52 μmol/L from May to September and 81 μmol/L for the second group, respectively. According to Eq. (2), the F value is 1.47. The Cl_{ref} are 76 μmol/L for May to September and 119 μmol/L for October to April, respectively. The latter high value is very close to the lowest Cl^- concentration (106 μmol/L) of river waters within the Lake Qinghai catchment (Zhang et al., 2009).

The calculated contributions show that rain input accounts for average 22% of total riverine cations in both rivers, with their values ranging from 18% to 24% in the Buha River and from 16% to 33% in the Shaliu River, respectively (Table 4). In addition, both rivers show increased rain contribution during the monsoon periods. It is noticed that one Shaliu River sample collected on 19th July has exclusive high rain contribution (33%), which is attributed to a heavy rain occurred on 16th July, resulting in a highest daily discharge in the year. These results further suggest that river waters are diluted during monsoon seasons and that atmospheric input contributes an important fraction to river water in the semi-arid areas.

4.4.2. Evaporite contribution

Assuming that all Cl^- after atmospheric correction comes from halite and all SO_4^{2-} from gypsum/anhydrite, the calculated average contributions of halite dissolution are 9% (5–12%) in the Buha River and 2% (0.8–5%) in the Shaliu River, respectively (Table 4), and the average gypsum contributions are 10% (5–14%) in the Buha River and 8% (4–16%) in the Shaliu River, respectively. Sulfate could also be generated via oxidation of pyrites (see Section 4.4.4) and therefore this estimate of SO_4^{2-} marks an upper limit of gypsum. These results indicate that although the sources of SO_4^{2-} have some uncertainties, the halite contribution is much higher in the Buha River than in the Shaliu River, in agreement with its dominant marine lithology.

4.4.3. Silicate contribution

Aluminosilicate and Ca–Mg silicate weathering can provide Ca^{2+}, Mg^{2+}, Na^+, and K^+ to river waters. If all Na^* after rain and halite correction is silicate-derived ($Na_{sil} = Na_r - Na_{rain} - Na_{hal}$), the silicate contributions of Ca^{2+} and Mg^{2+} (Ca_{sil}, Mg_{sil}) are calculated assuming that both are released to rivers from silicates in a fixed proportion relative to Na^*. For our study, the average $(Ca/Na)_{sil}$ and $(Mg/Na)_{sil}$ ratios measured in silicate rocks are 0.47 ± 0.19 and 0.38 ± 0.11 in the Buha River catchment, and 0.48 ± 0.43 and 0.45 ± 0.16 in the Shaliu River catchment, respectively (Table 3). These ratios are based on 27 and 6 rock samples in the Buha and Shaliu River catchments, respectively, including granites, clastic rock, schist, sandstones, and high-grade metamorphic rocks. Then the fractions of cation contributions derived from the silicates to the rivers are calculated. Within the uncertainties of the $(Ca/Na)_{sil}$ and $(Mg/Na)_{sil}$ ratios, the average silicate contributions are 8 ± 2% (2–18%) in the Buha River and 20 ± 5% (11–31%) in the Shaliu River, respectively (Table 4). It is obvious that contribution of silicate weathering in the Shaliu River is approximately two times higher than that in the Buha River, which is consistent with different lithologic distribution in each river catchment.

4.4.4. Carbonate contribution

In calculating carbonate contribution to rivers, it is important to isolate contribution of gypsum-derived SO_4^{2-} from that via pyrite oxidation, as the latter can supply protons from H_2SO_4 weathering without consuming atmospheric CO_2. Generally, pyrite oxidation would result in high Si and SO_4^{2-} but low HCO_3^- concentrations (Huh et al., 1998a,b). However, both the Buha and Shaliu Rivers exhibit low Si and SO_4^{2-} but high HCO_3^- contents, thus SO_4^{2-} may mainly originate from gypsum dissolution. Assuming that all SO_4^{2-} is from gypsum dissolution and considering the uncertainties of the $(Ca/Na^*)_{sil}$ and $(Mg/Na^*)_{sil}$ ratios, the average carbonate contributions are 52 ± 2% (45–58%) in the Buha River and 46 ± 5% (31–63%) in the Shaliu River, respectively (Table 4). These are lower limits of carbonate contributions for both catchments.

If all SO_4^{2-} is from oxidation of pyrite, the upper limits of carbonate contributions are 60 ± 2% (52–65%) in the Buha River and 55 ± 5% (47–67%) in the Shaliu River, respectively. It is noted that the river waters are supersaturated with respect to calcite in both the Buha and Shaliu Rivers (CSI > 0, Table 1), thus some Ca^{2+} might be removed by calcite precipitation, resulting in underestimating the carbonate contribution. In any case, carbonate weathering has contributed more than half of total cations to the waters of both rivers.

Although limited limestone outcrops within the Shaliu River catchment, Ca^{2+} and HCO_3^- dominate the water chemistry as in the Buha River. It has been shown that in some silicate-dominated watersheds, weathering of trace amounts of calcite may contribute a significant amount of Ca^{2+} and HCO_3^- (Blum et al., 1998; Jacobson et al., 2003; Oliva et al., 2004; Hagedorn and Cartwright, 2009).

4.5. Rates of CO_2 consumption by silicate weathering

The rate of net CO_2 consumption by silicate weathering ($ØCO_2$) is calculated based on the silicate cations, coupled with the data of drainage areas (A) and weekly averaged water discharges (Q).

$$ØCO_2 = Ø(K_{sil} + Na_{sil} + 2 \times Ca_{sil} + 2 \times Mg_{sil}) \times Q/A \quad (3)$$

For some springtime samples with abnormally high Na^+ and Cl^- contents in the Buha River that might be affected by eolian dust (Jin et al., 2011), we use $ØCO_2 = 2ØSi$ instead (Edmond and Huh, 1997) because the dissolved fluxes from eolian dust are unknown and Si is conservative in the springtime river waters. It has been reported that independent estimate of $ØCO_2$ can be made from Si concentrations, especially in those areas where carbonates and evaporates are abundant (Hagedorn and Cartwright, 2009 and references therein). The time series $ØCO_2$ data within the Buha and Shaliu River catchments are listed in Table 4.

The annual $ØCO_2$ is $282 \pm 71 \times 10^3$ mol/km^2/yr in the Shaliu River catchment and $19 \pm 3 \times 10^3$ mol/km^2/yr in the Buha River catchment, respectively. These values are their upper limits, since pyrite oxidation generates H_2SO_4 that can weather silicate minerals without consuming atmospheric CO_2. If all the SO_4^{2-} is from pyrite oxidation and is consumed by silicate weathering, the recalculated $ØCO_2$ would decrease to 171×10^3 mol/km^2/yr in the Shaliu River catchment and nearly all the values would be negative in the Buha River catchment. Obviously, the latter assumption is unreasonable for the Buha River and provides only a reference of a lower limit of $ØCO_2$ for the Shaliu River, because carbonate will preferentially consume most of H_2SO_4 relative to silicates (Chou et al., 1989). Tranter et al. (2002) proposed that only trace quantities (~0.7%) of carbonate and sulfides in silicate bedrock surface could dissolve five times more carbonate than silicate. Therefore, in our study areas where carbonate weathering dominates water chemistry, the pyrite oxidation would not apparently affect the $ØCO_2$, even assuming that pyrite does exist in the Buha and Shaliu River catchments.

For the seasonal variations of $ØCO_2$, it is observed that $ØCO_2$ varies from 4 mol/km^2/yr in the dry season to 3687 mol/km^2/yr in the monsoon season in the Shaliu River, and from 1 mol/km^2/yr in the dry season to 229 mol/km^2/yr in the monsoon in the Buha River, respectively (Table 4).

Table 4
Chemical weathering fluxes and net CO_2 consumption rates for the Shaliu River and Buha River catchments.

Sample no.	Date (mm/dd/yy)	Discharge[a] (m^3/s)	T[b] (°C)	Silicate	Carbonate	Rain	Halite	Gypsum	SWR[c] (kg/km^2/day)	PER[d] (kg/km^2/day)	Net ØCO_2 (mol/km^2/day)
				% of Cations							
Shaliu River catchment											
SL09-01	01/04/09	0.91	−18.0	20	33	18	12	18	1.5	–	70
SL09-02	01/11/09	0.78	−21.0	28	30	17	13	13	1.6	–	83
SL09-03	01/18/09	0.32	−17.0	28	31	16	12	12	0.7	–	37
SL09-04	01/25/09	0.16	−14.5	28	30	17	12	12	0.3	–	17
SL09-05	02/01/09	0.15	−11.0	27	30	17	13	13	0.3	–	15
SL09-06	02/08/09	0.11	−13.0	17	33	17	13	19	0.1	–	7
SL09-07	02/15/09	0.12	−9.0	11	56	21	5	8	0.1	–	4
SL09-08	02/22/09	0.12	−13.0	16	51	15	8	10	0.2	–	8
SL09-09	03/01/09	0.19	−10.0	25	27	22	11	15	0.3	–	14
SL09-10	03/08/09	0.21	−13.0	10	56	23	4	7	0.1	–	6
SL09-11	03/15/09	0.25	−12.0	14	53	15	8	10	0.3	–	16
SL09-12	03/22/09	0.29	−3.5	24	29	22	11	14	0.4	–	21
SL09-13	03/29/09	1.74	−7.0	16	45	25	5	9	1.5	–	76
SL09-14	04/05/09	2.38	−6.5	17	44	25	5	9	2.1	–	104
SL09-15	04/12/09	4.40	2.0	11	57	20	4	8	3.3	–	166
SL09-16	04/19/09	4.49	0.5	14	47	30	2	7	2.7	–	135
SL09-17	04/26/09	3.93	0.5	13	51	27	2	6	2.5	–	125
SL09-18	05/03/09	2.95	0.0	19	47	22	3	8	2.6	1.8	133
SL09-19	05/10/09	3.29	4.0	16	51	23	3	7	2.4	3.8	120
SL09-20	05/17/09	2.87	1.0	20	45	25	1	9	2.4	2.4	122
SL09-21	05/24/09	2.39	1.5	20	46	25	1	8	2.0	2.0	102
SL09-22	05/31/09	8.76	4.0	21	46	26	0	8	7.2	135.1	371
SL09-23	06/07/09	4.34	5.0	20	46	26	1	8	3.5	4.4	180
SL09-24	06/14/09	6.35	7.0	20	46	25	1	8	5.2	11.1	269
SL09-25	06/21/09	19.35	7.0	20	46	26	1	7	15.5	199.3	796
SL09-26	06/28/09	27.87	7.0	20	46	25	1	8	22.6	256.6	1161
SL09-27	07/05/09	26.41	10.0	19	47	25	1	8	20.6	135.4	1059
SL09-28	07/12/09	44.64	9.0	20	46	25	1	8	36.5	488.0	1879
SL09-29	07/19/09	53.41	11.0	12	49	33	0	5	22.4	2432.4	1046
SL09-30	07/26/09	39.13	8.5	21	48	23	0	8	35.2	206.4	1823
SL09-31	08/02/09	30.50	10.0	21	48	23	1	7	28.6	252.9	1481
SL09-32	08/09/09	39.17	5.0	17	52	22	1	7	31.5	236.3	1605
SL09-33	08/16/09	20.11	7.0	19	51	21	1	8	18.4	29.3	950
SL09-34	08/23/09	27.67	9.0	–	–	–	–	–	–	103.0	–
SL09-35	08/30/09	35.34	4.5	27	39	24	1	10	40.8	92.9	2099
SL09-36	09/06/09	25.71	10.0	22	50	18	2	8	32.5	62.9	1684
SL09-37	09/13/09	47.60	6.0	24	49	16	2	9	71.4	719.5	3687
SL09-38	09/20/09	63.76	4.0	29	35	18	4	13	110.1	639.9	5512
SL09-39	09/27/09	32.39	2.0	31	31	17	5	16	60.0	131.0	3096
SL09-40	10/04/09	20.84	−1.0	27	39	20	3	10	35.3	51.8	1823
SL09-41	10/11/09	19.39	−3.0	28	36	21	3	12	32.7	10.1	1653
SL09-42	10/18/09	16.54	−4.5	25	42	22	2	9	23.6	6.7	1219
SL09-43	10/25/09	13.34	−6.0	24	44	19	3	10	21.9	–	1129
SL09-44	11/01/09	11.67	−10.0	24	43	21	2	9	17.3	–	892
SL09-45	11/08/09	9.69	−7.0	27	35	21	3	15	16.2	–	820
SL09-46	11/15/09	5.60	−10.0	24	46	19	2	9	8.7	–	448
SL09-47	11/22/09	3.55	−17.5	15	58	20	2	5	3.4	–	174
SL09-48	11/29/09	3.18	−15.0	15	58	20	3	5	3.2	–	158
SL09-49	12/06/09	2.98	−17.0	11	62	21	1	4	2.1	–	104
SL09-50	12/13/09	2.66	−14.0	11	62	21	1	4	1.8	–	93
SL09-51	12/20/09	2.45	−20.5	11	63	19	3	4	1.9	–	94
SL09-52	12/27/09	2.15	−22.5	12	62	20	2	5	1.7	–	84
SL09-53	01/04/10	2.06	−15.5	12	62	20	2	5	1.6	–	79
Buha River catchment											
BH07-01	01/01/07	2.19	−15.0	9	53	22	8	8	0.1	–	6
BH07-02	01/07/07	2.07	−13.5	15	46	22	9	8	0.2	–	10
BH07-03	01/14/07	1.90	−15.0	10	53	22	8	7	0.1	–	6
BH07-04	01/21/07	1.79	−15.0	2	58	22	11	7	0.0	–	1
BH07-05	01/28/07	1.77	−14.5	10	52	22	8	8	0.1	–	5
BH07-06	02/04/07	1.80	−9.5	9	53	23	8	8	0.1	–	5
BH07-07	02/11/07	1.67	−11.0	18	50	23	5	5	0.2	–	9
BH07-08	02/18/07	1.66	−19.5	10	53	23	7	7	0.1	–	5
BH07-09	02/25/07	1.65	−11.5	n. c.	n. c.	n. c.	n. c.	n. c.	n. c.	–	3
BH07-10	03/04/07	1.59	−13.5	n. c.	n. c.	n. c.	n. c.	n. c.	n. c.	–	3
BH07-11	03/11/07	1.70	−4.5	n. c.	n. c.	n. c.	n. c.	n. c.	n. c.	–	3
BH07-12	03/18/07	1.60	−12.0	n. c.	n. c.	n. c.	n. c.	n. c.	n. c.	–	3
BH07-13	03/25/07	1.62	−11.5	n. c.	n. c.	n. c.	n. c.	n. c.	n. c.	–	2
BH07-14	04/01/07	1.92	−5.5	n. c.	n. c.	n. c.	n. c.	n. c.	n. c.	–	3
BH07-15	04/08/07	2.25	1.5	n. c.	n. c.	n. c.	n. c.	n. c.	n. c.	–	3
BH07-16	04/15/07	2.12	−5.5	n. c.	n. c.	n. c.	n. c.	n. c.	n. c.	–	3
BH07-17	04/22/07	3.80	−0.5	n. c.	n. c.	n. c.	n. c.	n. c.	n. c.	–	6

(*continued on next page*)

Table 4 (*continued*)

Sample no.	Date (mm/dd/yy)	Discharge[a] (m^3/s)	T[b] (°C)	Silicate	Carbonate	Rain	Halite	Gypsum	SWR[c] (kg/km^2/day)	PER[d] (kg/km^2/day)	Net $ØCO_2$ (mol/km^2/day)
				% of Cations							
BH07-18	04/29/07	5.42	2.5	n. c.	n. c.	n. c.	n. c.	n. c.	n. c.	0.1	8
BH07-19	05/06/07	4.99	3.0	n. c.	n. c.	n. c.	n. c.	n. c.	n. c.	0.2	7
BH07-20	05/13/07	8.81	−2.5	n. c.	n. c.	n. c.	n. c.	n. c.	n. c.	1.9	12
BH07-21	05/20/07	4.91	3.0	n. c.	n. c.	n. c.	n. c.	n. c.	n. c.	0.3	6
BH07-22	05/27/07	3.47	4.0	n. c.	n. c.	n. c.	n. c.	n. c.	n. c.	0.1	4
BH07-23	06/03/07	2.79	7.0	n. c.	n. c.	n. c.	n. c.	n. c.	n. c.	0.2	4
BH07-24	06/10/07	2.31	5.5	8	54	23	6	9	0.1	0.2	4
BH07-25	06/17/07	4.67	11.5	5	55	23	7	9	0.1	2.6	6
BH07-26	06/24/07	62.21	6.5	11	55	22	5	7	3.3	498.6	156
BH07-27	07/01/07	52.79	13.5	5	58	24	6	8	1.4	66.1	62
BH07-28	07/08/07	70.30	9.0	6	54	24	7	9	2.1	257.5	93
BH07-29	07/15/07	43.31	15.5	5	58	24	6	7	1.1	28.9	49
BH07-30	07/22/07	104.43	9.5	8	51	21	8	12	4.6	698.2	210
BH07-31	07/29/07	66.90	12.0	9	47	21	9	13	3.4	88.8	158
BH07-32	08/05/07	40.37	9.5	10	48	20	9	12	2.2	21.5	108
BH07-33	08/12/07	50.03	11.0	10	48	21	9	12	2.7	38.0	126
BH07-34	08/19/07	42.67	13.0	5	53	19	10	14	1.3	24.5	57
BH07-35	08/26/07	107.76	8.0	5	54	18	9	14	3.6	464.0	155
BH07-36	09/02/07	152.29	11.5	5	56	18	9	13	4.7	472.0	209
BH07-37	09/09/07	116.84	4.5	6	52	19	9	14	4.0	81.1	181
BH07-38	09/16/07	157.14	1.5	5	53	19	9	14	5.1	403.7	229
BH07-39	09/23/07	92.70	8.0	5	54	19	9	14	3.2	59.6	143
BH07-40	09/30/07	91.84	0.0	5	54	19	9	14	2.8	81.0	123
BH07-41	10/07/07	89.21	0.0	4	53	22	8	12	2.6	40.8	113
BH07-42	10/14/07	78.66	−1.0	3	53	23	9	12	1.8	13.6	73
BH07-43	10/21/07	55.47	2.5	4	53	23	8	12	1.6	3.8	71
BH07-44	10/28/07	39.39	−5.0	5	53	22	9	12	1.3	0.4	56
BH07-45	11/04/07	22.27	−6.5	14	45	22	10	8	1.9	–	93
BH07-46	11/11/07	16.56	−10.5	14	45	22	11	8	1.4	–	68
BH07-47	11/18/07	14.23	−9.5	8	52	22	8	10	0.7	–	32
BH07-48	11/25/07	8.72	−11.0	9	52	23	8	9	0.5	–	22
BH07-49	12/02/07	4.54	−14.5	8	51	24	8	9	0.2	–	10
BH07-50	12/09/07	3.59	−13.0	9	51	24	8	9	0.2	–	9
BH07-51	12/16/07	3.16	−19.5	8	51	24	8	9	0.1	–	7
BH07-52	12/23/07	3.15	−9.0	7	51	24	8	9	0.1	–	6
BH07-53	12/30/07	2.74	−20.5	8	51	24	8	9	0.1	–	6

n.c. – Refers to not calculated, since the samples might be significantly affected by potential dust input.
"–" refers to lack of data.
[a] Discharge is weekly average.
[b] *T* refers to mean daily air temperature.
[c] SWR refers to silicate weathering rate calculated from silicate derived cations.
[d] Physical erosion rate = (weekly suspended particulate material flux)/7.

Generally, $ØCO_2$ has been calculated by using river water samples collected during the rainy season. In this study, the $ØCO_2$ calculated by rainy season samples are 16×10^3 mol/km^2/yr in the Buha River catchment and 182×10^3 mol/km^2/yr in the Shaliu River catchment, which are 16% and 35% lower than the annual $ØCO_2$ sum by all weekly samples in the respective catchment. Such obvious difference can be attributed to high silicate-derived cations in the dry seasons, owing to longer water–rock interaction relative to the running discharge during the rainy seasons.

4.6. Controls on silicate weathering rate (SWR) and $ØCO_2$

4.6.1. Lithology

The field meteorological data show that air temperature and precipitation exhibit very similar seasonal patterns between 2007 and 2009, with their high values during the monsoon seasons and low values during the dry seasons (Fig. 2). Under such same climatic conditions, the lithology control on $ØCO_2$ can be compared between the catchments. The calculation shows that in the Shaliu River, the annual $ØCO_2$ is 15 times higher than that in the Buha River, which can be attributed to the distinct lithology between the two catchments. The Buha River catchment is dominated by late Paleozoic marine limestone, whereas Triassic sandstone and Late Cambrian metamorphic rocks dominate within the Shaliu River catchment.

4.6.2. Water discharge and temperature

Among the climatic factors governing SWR, White and Blum (1995) proposed that precipitation, temperature and runoff dominate, whereas Dalai et al. (2002) indicated that temperature is most important and Turner et al. (2010) further observed a substantial temperature control in high rainfall and favorable topography conditions. In contrast, recent studies suggested that runoff plays a critical role on SWR (Singh et al., 2005; Tipper et al., 2006; Hren et al., 2007; Moon et al., 2007; Noh et al., 2009) and that there is no obvious effect by temperature (Huh and Edmond, 1999; Riebe et al., 2004; Hren et al., 2007; Hagedorn and Cartwright, 2009). Thus, the identification of these climatic controls on SWR remains a debate. In this study, one of the goals is to investigate whether there is a water discharge and/or temperature control on SWR in the semi-arid regions. If any, how about their relationship with monsoonal seasonality?

The correlations between seasonal $ØCO_2$ versus *Q* and air temperature are carried out in the Shaliu and Buha River catchments (Fig. 6) in order to test their controls on SWR. $ØCO_2$ is calculated as the product of *Q* and silicate-derived ions using Eq. (3). As the silicate-derived ions is much less variable than *Q* in both rivers,

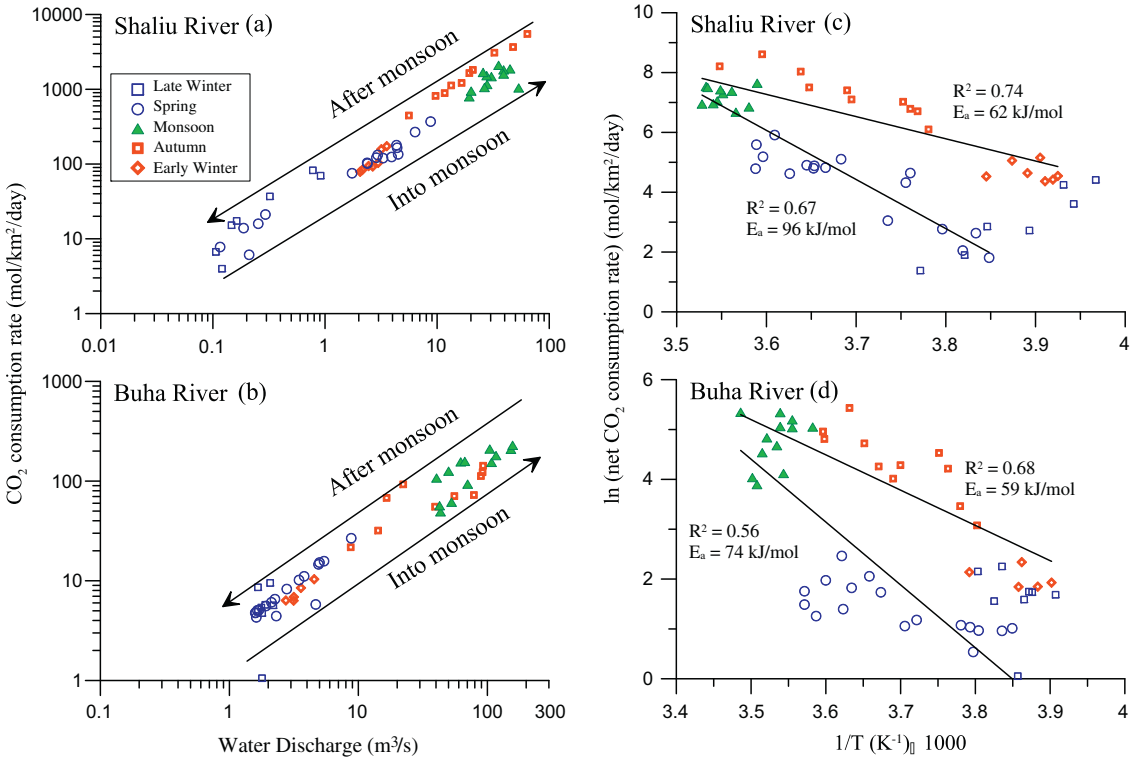

Fig. 6. Relationships between net CO_2 consumption rate ($ØCO_2$) versus water discharge and air temperature. A strong correlation of $ØCO_2$ and water discharge suggests the dominated control of discharge on silicate weathering (a and b). The two arrows mark the $ØCO_2$ change directions before and after the mid-monsoons (a and b). Air temperature exhibits two different trends with $ØCO_2$ in both the Shaliu River (c) and Buha River (d), i.e. before and after the mid-monsoons, indicating $ØCO_2$ dependence on temperature as well.

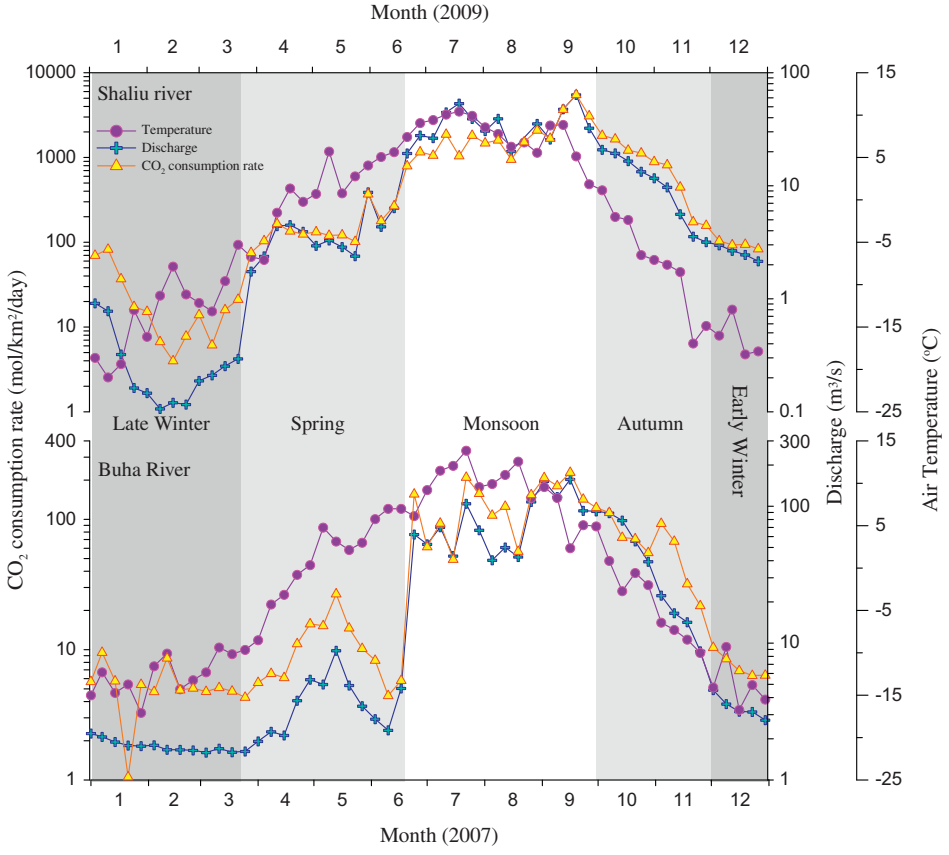

Fig. 7. The time-series variations of $ØCO_2$, air temperature and water discharge in the Shaliu and Buha Rivers, showing significant seasonal variations.

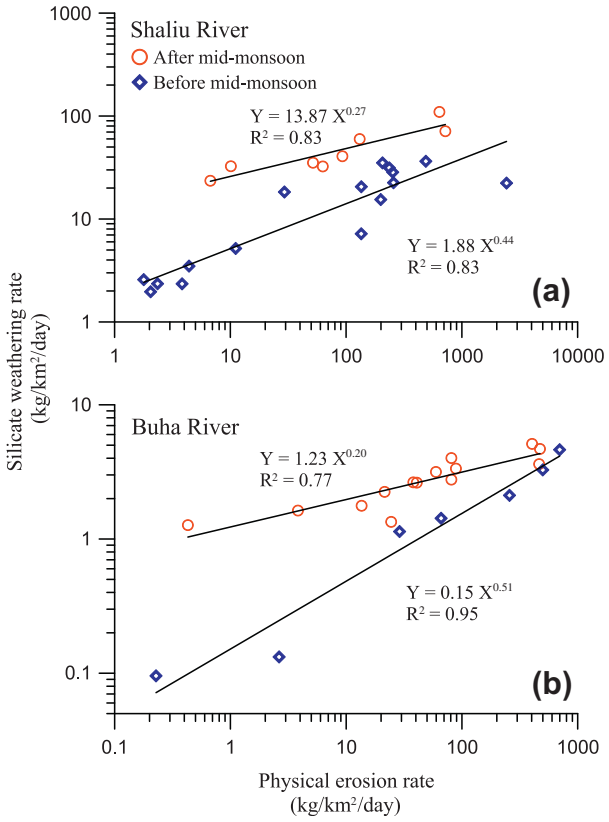

Fig. 8. Plots of physical erosion rate (PER) versus silicate weathering rate (SWR) in the Shaliu River (a) and the Buha River (b). Different power law functions between SWR and PER are observed in each river.

good linear log–log correlations with a near-zero intercept are observed between Q and $ØCO_2$ over a one year period (Fig. 6a, b), indicating a dominated control of Q on SWR in both river catchments.

Interestingly, different from the single relation obtained by seasonal samples collected in the Himalayas (Dalai et al., 2002) or by spatial samples from 68 small, mono-lithologic basins distributed around the world (White and Blum, 1995), air temperature in this study exhibits two distinct trends with $ØCO_2$ during 2 time periods in each catchment (Fig. 6c and d). It is noted that it may be misleading to believe that there is a weak correlation between temperature and $ØCO_2$, if the weekly $ØCO_2$ over a one year period is plotted with the air temperature ($R^2 = 0.30$ in the Shaliu River and $R^2 = 0.41$ in the Buha River), without seasonal classification. However, by classifying into before and after the mid-monsoons, the two trends are observed for both of the river catchments in Fig. 6c and d. The steeper slopes for before the mid-monsoons merely reflect the greater control of temperature on SWR and $ØCO_2$ relative to after the mid-monsoon.

During the winters, air temperature decreases to the lowest with its values below −10 °C in both catchments (Fig. 7). The precipitation is very low and is in the form of snow. The discharge might be sustained by subsurface flow and the $ØCO_2$ decreases to the lowest. During this period the catchment surface is frozen and is covered by ice and snow. From winter to monsoon seasons, air temperature gradually increases and the rivers are fed by melt-water of ice and snow, resulting in gradually increasing $ØCO_2$ (Fig. 7). It has been reported that the melt-water began to feed the discharge within the Lake Qinghai catchment in March, and the effect of melt-water would be diminishing in May because of the decreasing snow and increasing rainfall (LZBCAS, 1994). Also, this period are characterized by frequently dust storms. Therefore, during the period before the mid-monsoon, under a low discharge condition, increased silicate sources plausibly stem from (1) frozen soil, (2) groundwater, and/or (3) eolian dust input. After the mid-monsoon, although air temperature gradually decreases to −10 °C as before the mid-monsoon, high water discharge lasts a long period (Fig. 7), resulting in a relatively high $ØCO_2$ (Figs. 6c and d and 7). The two trends might suggest that temperature plays a more important role on the $ØCO_2$ before the mid-monsoon under a condition of low water discharge than that after the mid-monsoon when water discharge is high. In addition, the freezing erosion triggered by low temperature before the mid-monsoon also facilitates silicate weathering (discussed in Section 4.6.3). Under the low water discharge condition, therefore, the roles of temperature and physical erosion are augmented before the mid-monsoon relative to after the mid-monsoon. As a consequence, the combined effect of discharge, temperature and physical erosion produces the different trends before and after the mid-monsoons. The dominated control of Q on SWR and $ØCO_2$ is further supported by the lower slopes under high discharge after the mid-monsoon than that before the mid-monsoon, even at the rivers draining distinct lithology.

During the mid-monsoons, air temperature increases to about 15 °C and focused rainfall produces significantly increased discharge (Fig. 7). The highest $ØCO_2$ is observed during this period. It is found that the monsoonal $ØCO_2$ accounts for 75% and 71% of the total annual flux in the Shaliu and Buha River catchments, respectively, indicating dominant silicate weathering in the semi-arid northeastern Tibetan Plateau during the monsoons.

The two distinct trends between temperature and $ØCO_2$ can be further described by an Arrhenius relationship from which the activation energy (Ea) of the weathering reaction can be calculated (White and Blum, 1995; White et al., 1999). During the period

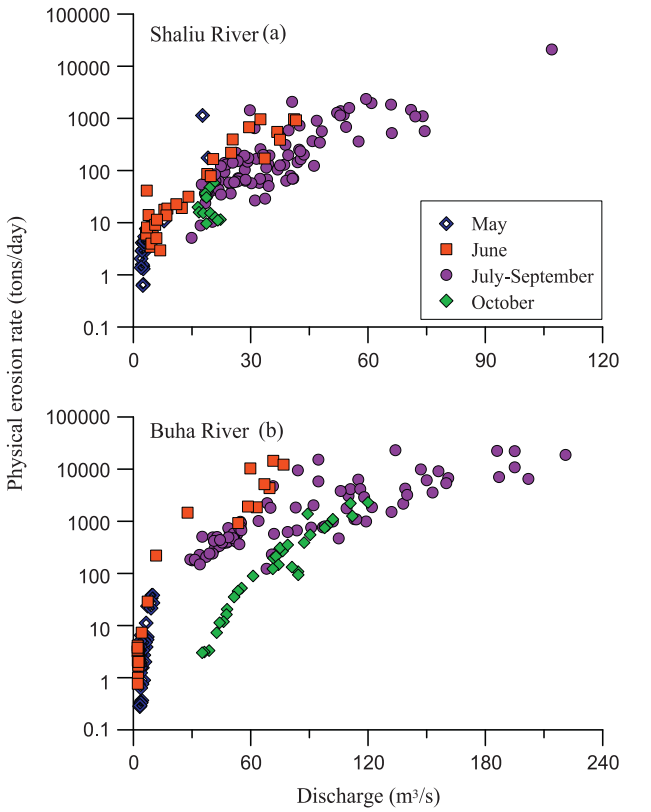

Fig. 9. Plots of physical erosion rate (PER) versus water discharge in the Shaliu and Buha Rivers (a and b). At a given discharge, the higher PER in May and June indicates the effects of frozen process and erosion of ice and snow.

before the mid-monsoons, the calculated Ea values of silicate weathering are 96 and 74 kJ/mol for the Shaliu and Buha River catchments, respectively, while after the mid-monsoon, the corresponding Ea are 62 and 59 kJ/mol, respectively. These values are within ranges obtained for silicate weathering in natural watersheds, such as 77 kJ/mol (Velbel, 1993), 69–78 kJ/mol (White and Blum, 1995), 51 kJ/mol (White et al., 1999), and 52–102 kJ/mol (Turner et al., 2010). According to laboratory weathering studies, easily weatherable minerals have lower Ea values, and different minerals have different Ea values. For example, the Ea derived from laboratory experiments is 25–35 kJ/mol for basaltic glass dissolution (Gislason and Eugster, 1987; Gislason and Oelkers, 2003), 60 kJ/mol for albite, and 80 kJ/mol for oligoclase (White and Blum, 1995 and references therein). Hence, the higher Ea values during the period before the mid-monsoons than after the mid-monsoons in our study can be related to a greater dissolution of uneasily weatherable minerals derived from (1) frozen soil, owing to both the long residence time under low discharge and the new reactive minerals exposure by freezing erosion before the monsoon, (2) groundwater that also has long residence time, and/or (3) eolian dust input.

Anyway, these results suggest that the seasonal variations of $ØCO_2$ in the semi-arid catchments can be explained by the covariation of Q and temperature because of their strong coupling with monsoons, behaving a cluster in highest $ØCO_2$ during the monsoon maximum (at the times of highest Q and temperature) (Fig. 6).

4.6.3. Physical erosion

The effect of physical erosion on SWR has long been the focus since the hypothesis that rapid erosion exposes fresh, highly reactive minerals and then enhances SWR. The test of this hypothesis has been sought to define a positive correlation between physical erosion and SWR (Gaillardet et al., 1999; Millot et al., 2002; West et al., 2005). So far, four relationships between them were reported in previous studies, as illustrated as (1) a linear relationship, (2) a power function relationship, (3) under supply-limited conditions, SWR is in linear increase with physical erosion, whereas under kinetically-limited conditions, the relationship becomes less linear, and (4) no correlation.

The data of PER listed in Table 4 are weekly averaged SPM fluxes for comparing with SWR. The SWR is calculated based on silicate derived cations above. Unlike the four relationships listed above, in our two study catchments, relationships between PER versus SWR also show two distinct trends during the periods before and after mid-monsoon (Fig. 8a and b). During each period, their relationships obey a power law function, implying that the silicate weathering is promoted by physical erosion through providing fresh mineral exposure. Note that the higher exponent for a power function means a faster increase of SWR at a given range of PER. The exponents of power function are 0.44 and 0.51 before mid-monsoon and are 0.27 and 0.20 after mid-monsoon in the Shaliu and Buha Rivers, respectively. In this study, the higher exponent values before the mid-monsoons in both rivers than that after the mid-monsoons indicate that SWR increases faster before the mid-monsoons than after the mid-monsoon. Because, as mentioned above, the frozen soil and the erosion of ice and snow before the mid-monsoons in both catchments yield: (1) large volumes of fine grained sediment, and (2) new reactive minerals exposure with high surface area, as illustrated in several studies (Anderson et al., 1997; Anderson, 2007). Such high reactive material accelerates silicate weathering.

A further evidence for the supply of this material can be observed in Fig. 9. It shows that at a given discharge, the PER is generally higher during early monsoon (from May to June) than during late monsoon (from July to October) in both river catchments. A reason for the higher PER is that large volumes of fine material produced by freezing erosion during the winter and spring seasons was flushed out at the onset of monsoonal rainfall. Frost-shattering and freezing processes produce the fracturing of rock and fine material as reported previously (e.g. Gaillardet et al., 1999; Huh and Edmond, 1999).

5. Conclusions

The major ion chemistry of weekly river water, daily SPM content and detailed hydrological data from the semi-arid northeastern Tibetan Plateau over a one year period have brought out the following observations.

The river chemistry, SPM and physical erosion rate exhibit significant seasonal variations in both the Buha and Shaliu Rivers. In the Shaliu River, weathering of trace amounts of calcite dominates the Ca^{2+} and HCO_3^- of the river water. Using the weekly time-series variations of Ca^{2+} and elemental ratios, the signal of carbonate precipitation is captured at the end of monsoon in this river. Thus, in the rivers that are supersaturated with respect to calcite, densely time-series sampling might provide an effective way to monitor the process of carbonate precipitation.

Although the two rivers share the same climate conditions, the distinct lithology leads to a 15 times difference of annual $ØCO_2$ between the two catchments. The linear correlations between Q and $ØCO_2$ indicate a dominated control of Q on SWR in both river catchments. Different from the previous studies, the relationship between temperature and $ØCO_2$ shows two distinct trends during the periods before and after the mid-monsoons for both rivers, indicating that temperature plays a more important role on $ØCO_2$ before the mid-monsoon under a condition of low water discharge than that after the mid-monsoon with a high water discharge. The two distinct trends between physical erosion rates and silicate weathering rates indicate that freezing erosion before the monsoon accelerates silicate weathering rates.

Acknowledgements

This work was financially supported by NSFC through Grant 41225015 and by National Basic Research Program of China (2013CB956402). We especially thank Zhu Yuxin in Nanjing Institute of Geography & Limnology, CAS and Zhang Ting in IEECAS, for their kind help and suggestions to sample analyses and laboratory work. Thanks to Shi Yuewei and Qiu Xinning in the Buha River Hydrology Station and Wu Yuanxiang in the Shaliu River Hydrology Station for their assistance with sample collection. Thanks are also extended to the editor and three reviewers for their thoughtful reviews and comments that substantially improved an earlier version of this manuscript.

References

Anderson, S.P., 2007. Biogeochemistry of glacial landscape systems. Annual Review of Earth and Planetary Sciences 35, 375–399.

Anderson, S.P., Drever, J.I., Humphrey, N.F., 1997. Chemical weathering in glacial environments. Geology 25, 399–402.

Berner, R.A., Kothavala, Z., 2001. GEOCARB III: a revised model of atmospheric CO_2 over phanerozoic time. American Journal of Science 301, 182–204.

Berner, R.A., Lasaga, A.C., Garrels, R.M., 1983. The carbonate–silicate geochemical cycle and its effect on atmospheric carbon dioxide over the past 100 millions years. American Journal of Science 284, 641–683.

Bethke, C.M., Yeakel, S., 2009. The Geochemist's Workbench Release 8.0: Reaction Modeling Guide. Illinois, University of Illinois, Champaign, p. 84.

Bian, Q.T., Liu, J.Q., Luo, X.Q., Xiao, J.L., 2000. Geotectonic setting, formation and evolution of Qinghai Lake, Qinghai, China. Seismology and Geology 22, 20–26 (in Chinese with English abstract).

Blum, J.D., Gazis, C.A., Jacobson, A.D., Chamberlin, C.P., 1998. Carbonate versus silicate weathering in the Raikhot watershed within the High Himalayan Crystalline Series. Geology 26, 411–414.

Bluth, G.J.S., Kump, L.R., 1994. Lithologic and climatic control of river chemistry. Geochimica Cosmochimica Acta 58, 2341–2359.

Chen, G.S., Chen, X.Q., Gou, X.J., 2008. Eco-environmental Protection and Restoration at the Lake Qinghai Catchment. Qinghai People Press, Qinghai (in Chinese).
Chou, L., Garrels, R.M., Wollast, R., 1989. Comparative study of the kinetics and mechanisms of dissolution of carbonate minerals. Chemical Geology 78, 269–282.
Clow, D.W., Mast, M.A., 2010. Mechanisms for chemostatic behavior in catchments: implications for CO_2 consumption by mineral weathering. Chemical Geology 269, 40–51.
Dalai, T.K., Krishnaswami, S., Sarin, M.M., 2002. Major ion chemistry in the headwaters of the Yamuna river system: chemical weathering, its temperature dependence and CO_2 consumption in the Himalaya. Geochimica Cosmochimica Acta 66, 3397–3416.
Das, A., Krishnaswami, S., Sarin, M.M., Pande, K., 2005. Chemical weathering in the Krishna Basin and Western Ghats of the Deccan Traps, India: rates of basalt weathering and their controls. Geochimica Cosmochimica Acta 69, 2067–2084.
Edmond, J.M., Huh, Y., 1997. Chemical weathering yields from basement and orogenic terrains in hot and cold climates. In: Ruddiman, W.F. (Ed.), Tectonic Uplift and Climate Change. Plenum Press, pp. 329–351.
Gabet, E.J., Mudd, S.M., 2009. A theoretical model coupling chemical weathering rates with denudation rates. Geology 37, 151–154.
Gaillardet, J., Dupré, B., Allègre, C.J., 1999. Global silicate weathering and CO_2 consumption rates deduced from chemistry of large rivers. Chemical Geology 159, 3–30.
Galy, A., France-Lanord, C., 1999. Weathering processes in the Ganges–Brahmaputra basin and the riverine alkalinity budget. Chemical Geology 159, 31–60.
Galy, A., France-Lanord, C., 2001. Higher erosion rates in the Himalaya: geochemical constraints on riverine fluxes. Geology 29, 23–26.
Gislason, S.R., Eugster, H.P., 1987. Meteoric water–basalt interactions. I: a laboratory study. Geochimica Cosmochimica Acta 51, 2827–2840.
Gislason, S.R., Oelkers, E.H., 2003. The mechanism, rates and consequences of basaltic glass dissolution: II. An experimental study of the dissolution rates of basaltic glass as a function of pH and temperature. Geochimica Cosmochimica Acta 67, 3817–3832.
Gislason, S.R., Oelkers, E.H., Eiriksdottir, E.S., Kardjilov, M.I., Gisladottir, G., 2009. Direct evidence of the feedback between climate and weathering. Earth and Planetary Science Letters 277, 213–222.
Grosbois, C., Négrel, Ph., Fouillac, C., Grimaud, D., 2000. Chemical and isotopic characterization of the dissolved load of the Loire River. Chemical Geology 170, 179–201.
Hagedorn, B., Cartwright, I., 2009. Climatic and lithologic controls on the temporal and spatial variability of CO_2 consumption via chemical weathering: an example from the Australian Victorian Alps. Chemical Geology 260, 234–253.
Hren, M.T., Chamberlain, C.P., Hilley, G.E., Blisniuk, P.M., Bookhagen, B., 2007. Major ion chemistry of the Yarlung Tsangpo–Brahmaputra river: chemical weathering, erosion, and CO_2 consumption in the southern Tibetan plateau and eastern syntaxis of the Himalaya. Geochimica Cosmochimica Acta 71, 2907–2935.
Huh, Y., Edmond, J.M., 1999. The fluvial geochemistry of the rivers of Eastern Siberia: III. Tributaries of the Lena and Anabar draining the basement terrain of the Siberian Craton and the Trans-Baikal Highlands. Geochimica Cosmochimica Acta 63, 967–987.
Huh, Y., Tsoi, M.Y., Zaitsev, A., Edmond, J.M., 1998a. The fluvial geochemistry of the rivers of Eastern Siberia: I. Tributaries of the Lena River draining the sedimentary platform of the Siberian Craton. Geochimica Cosmochimica Acta 62, 1657–1676.
Huh, Y., Panteleyev, G., Babich, D., Zaitsev, A., Edmond, J.M., 1998b. The fluvial geochemistry of the rivers of Eastern Siberia: II. Tributaries of the Lena, Omoloy, Yana, Indigirka, Kolyma, and Anadyr draining the collisional/accretionary zone of the Verkhoyansk and Cherskiy ranges. Geochimica Cosmochimica Acta 62, 2053–2075.
Jacobson, A.D., Blum, J.D., Chamberlain, C.P., Craw, D., Koons, P.O., 2003. Climatic and tectonic controls on chemical weathering in the New Zealand Southern Alps. Geochimica Cosmochimica Acta 67, 29–46.
Jin, Z.D., You, C.F., Yu, J.M., Wu, L.L., Zhang, F., Liu, H.C., 2011. Seasonal contributions of catchment weathering and eolian dust to river water chemistry, northeastern Tibetan Plateau: chemical and Sr isotopic constraints. Journal of Geophysical Research – Earth Surface. http://dx.doi.org/10.1029/ 2011JF002002.
Lanzhou Branch of Chinese Academy of Sciences (LZBCAS), 1994. Evolution of Recent Environment in Qinghai Lake and Its Prediction. West Center of Resource and Environment, Chinese Academy of Sciences. Science Press, Beijing (in Chinese).
Meybeck, M., 1983. Atmospheric inputs and river transport of dissolved substances. In: Dissolved Loads of Rivers and Surface Quality/Quantity Relationships, vol. 141. IAHS Publication, pp. 173–192.
Meybeck, M., 1986. Composition chimique des ruisseaux non pollués de France. Sciences Géologiques–Bulletin 39, 3–77.
Millot, R., Gaillardet, J., Dupré, B., Allègre, C.J., 2002. The global control of silicate weathering rates and the coupling with physical erosion: new insights from rivers of the Canadian Shield. Earth and Planetary Science Letters 196, 83–98.
Moon, S., Huh, Y., Qin, J.H., Nguyen, V.P., 2007. Chemical weathering in the Hong (Red) River basin: rates of silicate weathering and their controlling factors. Geochimica Cosmochimica Acta 71, 1411–1430.
Noh, H., Huh, Y., Qin, J.H., Ellis, A., 2009. Chemical weathering in the Three Rivers region of Eastern Tibet. Geochimica Cosmochimica Acta 73, 1857–1877.
Oliva, P., Dupré, B., Martin, F., Viers, J., 2004. The role of trace minerals in chemical weathering in a high-elevation granitic watershed (Estibere, France): chemical and mineralogical evidence. Geochimica Cosmochimica Acta 68, 2223–2243.
Qin, J.H., Huh, Y., Edmond, J.M., Du, G., Ran, J., 2006. Chemical and physical weathering in the Min Jiang, a headwater tributary of the Yangtze River. Chemical Geology 227, 53–69.
Riebe, C.S., Kirchner, J.W., Finkel, R.C., 2003. Long-term rates of chemical weathering and physical erosion from cosmogenic nuclides and geochemical mass balance. Geochimica Cosmochimica Acta 67, 4411–4427.
Riebe, C.S., Kirchner, J.W., Granger, D.E., Finkel, R.C., 2004. Erosional and climatic effects on long-term chemical weathering rates in granitic landscapes spaning diverse climate regimes. Earth and Planetary Science Letters 224, 547–562.
Singh, S.K., Sarin, M.M., France-Lanord, C., 2005. Chemical erosion in the eastern Himalaya: major ion composition of the Brahmaputra and $\delta^{13}C$ of dissolved inorganic carbon. Geochimica Cosmochimica Acta 69, 3573–3588.
Stallard, R.F., Edmond, J.M., 1981. Geochemistry of the Amazon 1 Precipitation chemistry and the marine contribution to the dissolved load at the time of peak discharge. Journal of Geophysical Research 86 (C10), 9844–9858.
Tipper, E.T., Bickle, M.J., Galy, A., West, A.J., Pomiès, C., Chapman, H.J., 2006. The short term climatic sensitivity of carbonate and silicate weathering fluxes: insight from seasonal variations in river chemistry. Geochimica Cosmochimica Acta 70, 2737–2754.
Tranter, M., Sharp, M.J., Lamb, H.R., Brown, G.H., Hubbard, B.P., Willis, I.C., 2002. Geochemical weathering at the bed of Haut Glacier d'Arolla, Switzerland – a new model. Hydrological Processes 16, 959–993.
Turner, B.F., White, A.F., Brantley, S.L., 2010. Effects of temperature on silicate weathering: solute fluxes and chemical weathering in a temperate rain forest watershed, Jamieson Creek, British Columbia. Chemical Geology 269, 62–78.
Vance, D., Bickle, M., Ivy-Ochs, S., Kubik, P.W., 2003. Erosion and exhumation in the Himalaya from cosmogenic isotope inventories of river sediments. Earth and Planetary Science Letters 206, 273–288.
Velbel, M.A., 1993. Temperature dependence of silicate weathering in nature: how strong of a negative feedback on long term accumulation of atmospheric CO_2 and global greenhouse warming? Geology 21, 1059–1062.
Viers, J., Dupré, B., Braun, J.J., Deberdt, S., 2000. Major and trace element abundances, and strontium isotopes in the Nyong basin rivers (Cameroon): constraints on chemical weathering processes and elements transport mechanisms in humid tropical environments. Chemical Geology 169, 211–241.
Walker, J.C.G., Hays, P.B., Kasting, J.F., 1981. A negative feedback mechanism for the long-term stabilization of Earth's surface temperature. Journal of Geophysical Research 86, 9776–9782.
West, A.J., Galy, A., Bickle, M., 2005. Tectonic and climatic controls on silicate weathering. Earth and Planetary Science Letters 235, 211–228.
White, A.F., Blum, A.E., 1995. Effects of climate on chemical weathering in watersheds. Geochimica Cosmochimica Acta 59, 1729–1747.
White, A.F., Blum, A.E., Bullen, T.D., Vivit, D.V., Schultz, M., Fitzpatrick, J., 1999. The effect of temperature on experimental and natural chemical weathering rates of granitoid rocks. Geochimica Cosmochimica Acta 63, 3277–3291.
Wolff-Boenisch, D., Gabet, E.J., Burbank, D.W., Langner, H., Putkonen, J., 2009. Spatial variations in chemical weathering and CO_2 consumption in Nepalese High Himalayan catchments during the monsoon season. Geochimica Cosmochimica Acta 73, 3148–3170.
Zhang, F., Jin, Z.D., Hu, G., Li, F.C., Shi, Y.W., 2009. Seasonally chemical weathering and CO_2 consumption flux of Lake Qinghai river system in the northeastern Tibetan Plateau. Environmental Earth Sciences 59, 297–313.